Coastal Engineering 159 (2020) 103714

Contents lists available at ScienceDirect

Coastal Engineering

journal homepage: http://www.elsevier.com/locate/coastaleng

Variations of wave parameter statistics as influenced by water depth in coastal and inner shelf areas

Jilian Xiong [a,b], Zai-Jin You [c,d], Jin Li [a], Shu Gao [e], Qing Wang [a], Ya Ping Wang [e,f,*]

[a] Ministry of Education Key Laboratory for Coast and Island Development, School of Geographic and Oceanographic Sciences, Nanjing University, Nanjing, 210093, China
[b] Virginia Institute of Marine Science, College of William & Mary, Gloucester Point, VA, 23062, USA
[c] Centre for Ports and Marine Safety, Dalian Maritime University, Dalian, 116026, China
[d] School of Civil Engineering, University of Queensland, St Lucia, 4702, Australia
[e] State Key Laboratory of Estuarine and Coastal Research, School of Marine Sciences, East China Normal University, Shanghai, 200241, China
[f] Laboratory for Marine Geology, Qingdao National Laboratory for Marine Science and Technology, Qingdao, 266061, China

ARTICLE INFO

Keywords:
Wave height
Orbital velocity
Breaking waves
Rayleigh function
Weibull distribution
Linear wave theory
Intertidal flats
Inner shelf waters

ABSTRACT

Wave height, pressure and orbital velocity statistics, as influenced by the factor of water depth, are analyzed on the basis of five data sets collected *in situ* from two intertidal sites with a mean water depth of 0.8–2.7 m and three inner shelf sites (water depths 14.6–27.6 m). Acoustic Doppler Velocimeters (ADVs) were used to measure instantaneous wave pressure and current velocity at 0.20–0.35 m above sea bed. The zero-crossing wave analysis method was applied to analyze the wave data to determine the wave pressure amplitude P and orbital velocity amplitude U of individual waves, together with the frequency of occurrence distributions of P and U, which are compared with the three commonly-used, classic Rayleigh, modified Rayleigh and Weibull distributions. It is found that the distribution of P is almost identical to that of U for each of the five study sites. The distributions of P and U for the intertidal flat sites fit the Weibull distribution better than the classic or modified Rayleigh ones, indicating a shallowness effect which is associated with finite-banded wind-wave spectra and possible wave breaking or near-bed turbulence. On the other hand, the distributions of P and U measured at the three inner shelf sites agree almost equally with the three distributions. With increasing water depth, the distributions of P and U are shown to reduce from the two-parameter Weibull distribution at the shallow intertidal sites to the classic Rayleigh at the deep-water sites. For coastal engineering applications, an empirical formula is proposed to estimate more accurately the significant wave height in intermediate coastal waters based on the surface water elevation data.

1. Introduction

Statistics of wave parameters such as wave height, period, dynamic pressure and orbital velocity are useful in designing coastal structures and assessing offshore platform safety (Battjes and Groenendijk, 2000; Silva et al., 2015). Field, laboratory and theoretical studies have been carried out to obtain such information for coastal waters with varied water depths (van Vledder, 1991; Elfrink et al., 2006; Wu et al., 2016). For these environmental settings, a "deep water" environment is defined by the criterion of $kh \geq \pi$, where h is the local water depth and k is the wave number; likewise, "intermediate water" is defined by $0.1\pi < kh < \pi$ and "shallow water" by $kh \leq 0.1\pi$ (You, 2008).

The Rayleigh distribution is a widely-adopted parametric descriptor of oceanic waves, as a classical theory to define the probability density function (pdf) of deep-water wave height in a narrow-banded sea, based on a Gaussian distribution of sea surface elevation (Longuet-Higgins, 1952; Battjes, 1974; Power et al., 2016). This theory was modified to the one-parameter Rayleigh distribution function, to account for finite wave spectral bandwidth, by introducing a scale parameter, which was found to agree nicely with field observations (Cartwright and Longuet-Higgins, 1956; Longuet-Higgins, 1952; Massel and Sobey, 2000). Subsequently, a more general scheme, i.e., the two-parameter Weibull distribution, was suggested to define the distribution of oceanic wave heights (Forristall, 1978). The transition from Rayleigh's distribution to Weibull's was first

* Corresponding author. State Key Laboratory of Estuarine and Coastal Research, School of Marine Sciences, East China Normal University, Shanghai, 200241, China.
E-mail address: ypwang@nju.edu.cn (Y.P. Wang).

https://doi.org/10.1016/j.coastaleng.2020.103714
Received 31 July 2019; Received in revised form 29 March 2020; Accepted 18 April 2020
Available online 26 April 2020

established in Baquerizo and Losada (1999) for the condition of sloping beaches. The wave height probability distribution is often reported to deviate from the Rayleigh distribution in shallow water environments due to wave shoaling and breaking (Dally, 1990, 1992; Goda, 2010). Although additional parameterizations of the distributional forms were proposed for the situations that waves propagate from deep to shallow waters (Glukhovskiy, 1966; Elfrink et al., 2006; Mai et al., 2011; Jadhav and Chen, 2013), the Rayleigh, modified Rayleigh and Weibull distributions have remained as the most commonly-used ones (You, 2009).

In contrast, the statistical distribution in terms of wave orbital velocity has been studied by few investigators, especially for shallow water conditions (Sultan, 1992; Wiberg and Sherwood, 2008). This distribution is often assumed to be the same as that for wave height, implying that the Rayleigh distribution can also be used here. However, such an assumption needs to be verified with extensive field data. Furthermore, studies are rare to investigate statistical characteristics of combined wind-wave and swell for different water depths, e.g., intertidal flats where the water depth is extremely shallow, with probable wave breaking due to the shallowness, and with enhanced bottom friction over the gentle bed slopes of $\tan\theta = 10^{-3}$–10^{-4} (Wang et al., 2013).

The main purpose of this study is, by analyzing extensive field data for instantaneous wave pressure and orbital velocity measured in intertidal and inner shelf environments, to investigate the effects of water depth h, together with the associated wave breaking and bottom turbulence, on the statistical distributions of both wave height and orbital velocity amplitudes. On such a basis, a semi-empirical formula is proposed to improve the calculations of the significant wave height for coastal and inner shelf waters.

2. Field data collection

2.1. Study sites

Field measurements of waves and currents were carried out at two intertidal sites (T1 and R2) and three inner shelf sites (X1, S1 and W1) (for location, see Fig. 1). The sites T1 and R2 are located at the upper-middle and lower part of the intertidal flat on the Jiangsu Coast, respectively, which were periodically inundated by semi-diurnal tides. The cross-shore tidalflat profile has a convex-up shape with a mean bed slope, $\tan\theta$, of 1/600, while the local bed slope at T1 is around 1/1600 (Yu et al., 2017). The sites X1, S1 and W1 are located in inner shelf areas, with water depths of 14.6–27.6 m.

In terms of the regional settings, the Yellow Sea is an epi-continental sea with an average water depth of 44 m (Liu, 1982), while the East China Sea is an open marginal sea, separated from the Pacific Ocean by the Ryukyu Islands and Taiwan Island, with a mean water depth of 72 m (Dong et al., 2011). Tides over the region are dominantly semidiurnal. A maximum tidal range on springs of 9.39 m has been recorded on the central Jiangsu Coast (Ding et al., 2014) and 9.0 m in the coastal region of Hangzhou Bay (Du et al., 2007). In the Yellow Sea, the tide is characterized by a progressive Poincare wave transmitted from the East China Sea, where the tidal wave mainly consists of a northwestward progressive wave (Xing et al., 2012).

The annual mean significant wave height H_s in the Yellow Sea is around 0.6 m, with wave periods ranging from 2.1 to 6.8 s (Yang et al., 2014). Extreme storm waves are generated by storms in winter and typhoons in summer in this region causing serious damage to coastal infrastructures and properties by inundating coastal land and degrading coastal ecosystems (You and Chen, 2018). In the East China Sea, the monthly mean wave height is 1.2 m in winter, and 0.9 m from April to June (Dong et al., 2011); the prevailing winds are mostly southerly-southeasterly in July to mid-September and become northerly-northeasterly until April of the following year. The monsoon winds generally weaken from the East China Sea towards the Yellow Sea (Lee and Liu, 2013).

2.2. Instrumentation and setup

The field data of instantaneous current velocities and wave pressures were collected for each of the study sites using an ADV, which was mounted on an instrumented tripod and located at a height of 0.20–0.35 m above sea bed (for the deployment detail, see Table 1). Both the high frequency current velocities and wave pressures data were averaged over a constant period of 0.5 s (which is large compared with turbulence scale, but small with regard to wave periods).

The sites T1 and R2, with mean water depths of 0.8 m and 2.7 m,

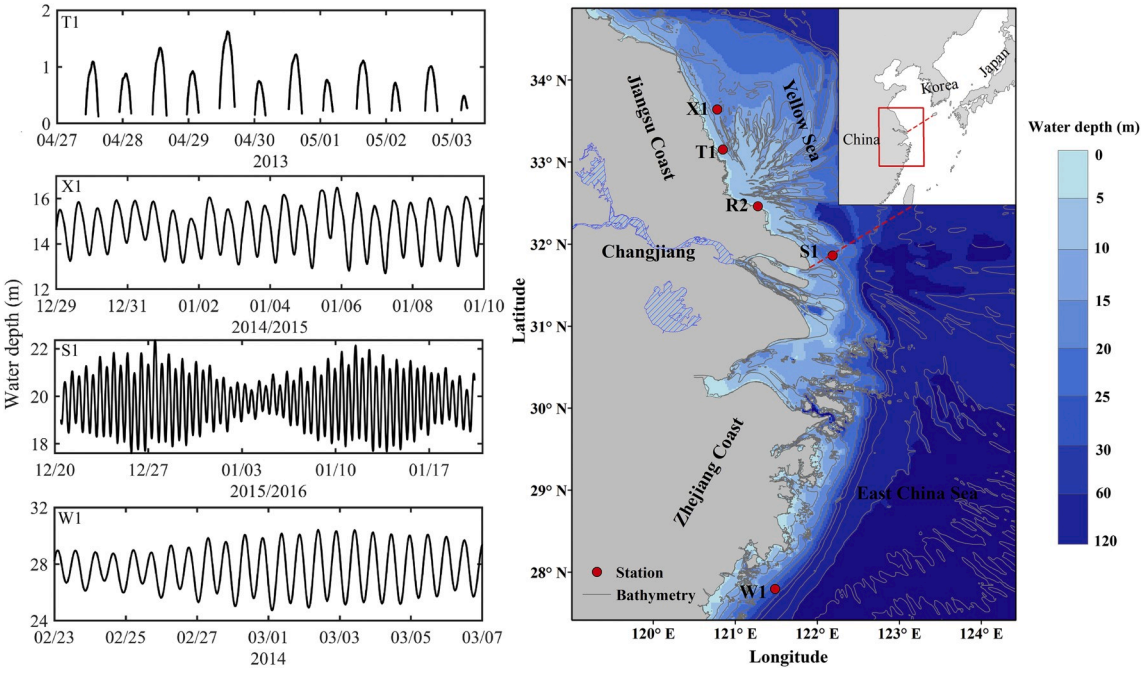

Fig. 1. The five study sites (X1, T1, R2, S1, W1) located in the coastal and inner shelf waters of mean depth $\overline{h}$ = 0.8–27.6 m, with the tidal water levels measured for the study sites.

Table 1
Deployment details and ADV setup.

Site	Mean Water Depth (m)	Sampling Rate (Hz)	Sampling Duration (s)	Sampling Interval (min)	Acoustic Sensor Elevation (m asb[a])	Deployment Duration (Day)
T1	0.8	8	30	1	0.20	7
R2	2.7	16	256	50	0.25	6
X1	14.6	16	512	10	0.35	13
S1	19.8	16	256	20	0.30	31
W1	27.6	16	512	30	0.30	16

[a] Note: asb = above sea bed.

respectively, during the measurement period, were periodically inundated by tides, whilst the other three sites (X1, S1, W1) had relatively large water depths (i.e., 14.6–27.6 m). The quality of the collected velocity data was first assessed by examining the velocity vector correlations being larger than 0.7 and signal-to-noise ratio being higher than 20 dB, and the outliers were replaced using the cubic interpolation method (Goring and Nikora, 2002; Lu et al., 2012). The wind speed and direction data at site T1 were obtained from the weather gauge stations at Sheyang City about 80 km to the northwest of the site (Yu et al., 2017).

An AXYS wave buoy, made in Canada by AXYS Technologies, was deployed at each of the inner shelf sites (X1, S1, and W1) to measure surface wave parameters and wind speeds/directions. The wave buoy recorded water surface elevations for 10 min in every hour (Xiong et al., 2018), and the surface buoy measurements were used to compare with the wave heights estimated from the ADV wave pressure data.

3. Wave data analyses

3.1. Wave pressure and amplitude

The zero-crossing wave analysis method in the time domain is used to analyze the collected instantaneous water pressure data to derive wave pressure amplitude P and wave period for individual waves. Instantaneous wave pressure $\tilde{p}$ is analyzed directly from the time series of instantaneous water pressure data as

$$\tilde{p}(t) = p(t) - \overline{p} \tag{1}$$

where $p(t)$ is the instantaneous water pressure recorded by ADV, and $\overline{p}$ is the mean water pressure averaged over one bust of sampling interval (Table 1). With the zero-crossing method, wave pressure amplitude P of individual wave is estimated as

$$P = 0.5 \times (P_{max} - P_{min}) \tag{2}$$

where $P_{\max}$ and $P_{\min}$ are maximum and minimum wave pressures, respectively, between two zero-up or -down crossing points. An example is shown in Fig. 2, where the P values are estimated from the field data collected at the site X1, with both the zero-up and -down crossing methods. The values of P estimated with the zero-up and -down crossing methods are shown to be close to each other; thus, the zero-up crossing method was then adopted in this study. Some other wave pressure characteristic parameters, i.e., significant wave pressure P_s, root-mean-squares wave pressure P_{rms} and maximum wave pressure P_{max}, are then derived from each burst of the wave pressure amplitudes analyzed. The wave height H was calculated from the wave pressure data collected in this study, based on the linear wave theory (Karimpour and Chen, 2017), the validity of which will be further discussed in section 5.2.

3.2. Wave orbital velocity and amplitude

Instantaneous wave orbital velocity components$(\tilde{u},\ \tilde{v})$ were determined from the measured instantaneous velocity components (u, v)

$$\tilde{u} = u - \overline{u} \text{ and } \tilde{v} = v - \overline{v} \tag{3}$$

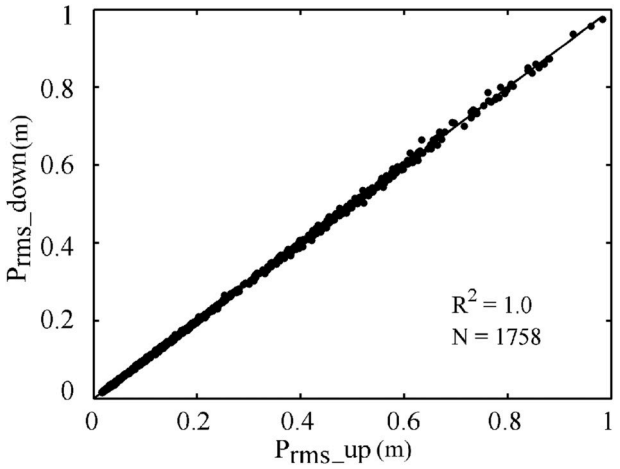

Fig. 2. Comparison of wave pressures P_{rms} calculated by the zero-up (P_{rms_up}) and zero-down (P_{rms_down}) crossing methods from 1758 bursts of wave pressure data collected at the site X1.

where $(\overline{u}, \overline{v})$ denote the mean eastern and northern velocity components averaged over each sampling duration, which varied from 30 to 512 s (Table 1), being much longer than the wave period. Thus, the tidal component was removed by using Eq (3) (Kim et al., 2000; MacVean and Lacy, 2014; Bian et al., 2018). However, the instantaneous wave orbital velocity components $(\tilde{u},\ \tilde{v})$, which were measured close to sea bed, may contain the turbulent velocity component, though the measured high frequency current velocities were averaged over a constant period of 0.5 s before the zero-crossing analysis. The influence of turbulence on the wave parameter statistics will be discussed in section 4.2. According to You and Yin (2001), the resultant wave orbital velocity $\tilde{U}(t)$ in the mean direction θ of wave propagation over one burst of sampling interval, during which the sea state is stationary, is expressed in terms of $\tilde{u}$ and $\tilde{v}$ as

$$\tilde{U}(t) = \tilde{u}\sin\theta + \tilde{v}\cos\theta \text{ and } \tan\theta = \pm\left(\frac{\tilde{u}_{rms}}{\tilde{v}_{rms}}\right) \tag{4}$$

where $\tilde{u}_{\rm rms}$ and $\tilde{v}_{\rm rms}$ are the root-mean-squares wave orbital velocity components that are directly calculated from one burst of instantaneous wave orbital velocities analyzed from Eq. (3). The histogram of $\tilde{u}/\tilde{u}_{\rm rms}$ and $\tilde{v}/\tilde{v}_{\rm rms}$ are found to be almost identical and perfectly follow the Gaussian distribution as commonly assumed, resulting from a stationary situation of $\tilde{u}/\tilde{u}_{\rm rms}$ and $\tilde{v}/\tilde{v}_{\rm rms}$ over the period of the deployment.

The wave orbital velocity amplitude U of individual waves can be analyzed from the time series of wave orbital velocity $\tilde{U}(t)$, with the zero-up crossing method. Similar to the definition of wave pressure amplitude in Eq. (2), U is estimated by

$$U = 0.5 \times (u_{max} - u_{min}) \tag{5}$$

where $u_{\max}$ and $u_{\min}$ are the maximum and minimum orbital velocity components of an arbitrary wave, respectively. Similar to the definition of irregular wave height, the wave orbital velocity parameters including

significant wave orbital velocity U_s, root-mean-squares wave orbital velocity U_{rms} and maximum wave orbital velocity amplitude U_{max} were then calculated from each burst record.

3.3. Wave period

In this study, wave period of an individual wave was analyzed from the time series of wave pressure data. The zero-up crossing period T_z is defined from the wave pressure data as the temporal interval between two consecutive zero-up crossing points on the x-axis of time. The mean wave period $\overline{T}_z$ for one burst of n waves is calculated by averaging n zero-up crossing periods analyzed from that data burst. The mean wave period is also estimated as $\overline{T}_m = \sqrt{m_0/m_2}$ from the wave spectrum, as calculated from each burst of wave pressure data (Jadhav and Chen, 2013; Karimpour and Chen, 2017), where m_0 and m_2 are the 0-th and second moments of the wave pressure spectrum, respectively.

The mean wave periods of $\overline{T}_z$ and $\overline{T}_m$ in Fig. 3, which were analyzed from the wave pressure data at the site X1, are shown to be close to each other, but quite different from those of peak wave period T_p corresponding to peak wave energy density. Since T_p is less stable than $\overline{T}_m$, only the $\overline{T}_z$ and $\overline{T}_m$ data were used in this study.

3.4. Wave characteristics with different water depths

The data on wind speed, mean wave period, significant wave pressure and significant orbital velocity, as analyzed from the field data collected at the study sites, are shown in Fig. 4. The probability density distribution of wave period $\overline{T}_z$ (Fig. 5), which is calculated from each of the study sites, was used to distinguish wind-waves of $\overline{T}_z$<5 s from swell of $\overline{T}_z \geq$5 s.

At the site T1 (water depth <1.5 m), the waves (measured at 0.2 m above the sea bed) are generally wind-waves of 1.5 s $\leq \overline{T}_z <$4 s (Fig. 5). The wave periods were clearly shown to increase or decrease during the rising or falling of the tides, respectively. Wave breaking took place during the strong wind period in April 29–30, under the condition of $h < 0.2$ m (Fig. 4). Some of the waves measured at this site belonged to shallow-water waves ($kh < 0.1\pi$), and the remainder belonged to transitional waves ($0.1\pi < kh < \pi$).

The waves at X1 (measured at 0.35 m above sea bed, $\overline{h} = 14.6$ m) represented a mixture of wind-waves (3 s $\overline{T}_z <$ 5 s) and swells (5 $\leq \overline{T}_z$ 9 s), but were generally dominated by 65% of swells (Fig. 5). Even though the wind-waves with short periods of $\overline{T}_z < 4\,s$ are generally classified as deep-water waves at this site ($kh > \pi$), the small wind-wave orbital velocities of $U_s <$ 8.3 cm/s were still detected by the ADV at 0.35 m above sea bed. Two storm events, which are marked in the shaded boxes in Fig. 4, generated the storm waves at this site. A small portion of the wind-waves measured at this site were deep-water waves ($kh \geq \pi$), and most of them are transitional waves ($0.1\pi < kh < \pi$).

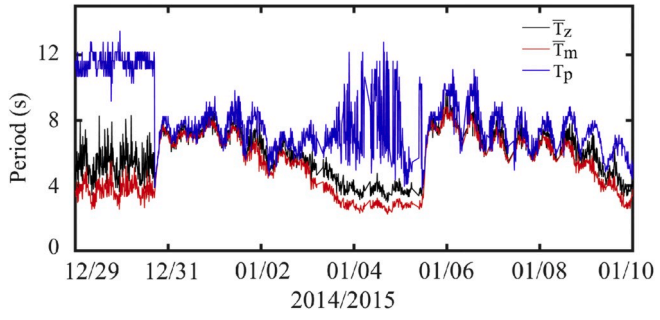

Fig. 3. Comparison of wave periods ($\overline{T}_z$, $\overline{T}_m$, T_p), as analyzed from wave pressure data collected at the site X1 with the zero-crossing and wave spectral methods.

At the sites S1 and W1 ($\overline{h}$ = 19.8 m and 27.6 m, respectively), the waves measured at 0.3 m above sea bed were all swells ($\overline{T}_z > 5\,s$). The wave periods at S1 were shorter than those at the site W1. All waves measured at the two sites belonged to transitional waves. It should be noted that the waves measured at 0.3 m above sea bed represented only the swells with a wave length that was sufficiently large to influence the bed, whilst the surface wind-waves were too short to reach the bed, during the measurements.

4. Statistical distributions of wave parameters

4.1. Probability distribution functions

Three commonly-used probability distribution functions, i.e., the Rayleigh, modified Rayleigh and Weibull distributions, were used here to evaluate the probability distributions of wave height and orbital velocity for different water depths. The Rayleigh function is expressed as

$$f(x) = 2x\exp\left(-x^2\right) \tag{6}$$

where x is the non-dimensional variable, e.g., $x = P/P_{rms}$ or $x = U/U_{\mathrm{rms}}$. In order to make the Rayleigh function flexible, a parameter was introduced in Eq. (6) to modify the Rayleigh as a one-parameter distribution (Longuet-Higgins, 1952; Massel and Sobey, 2000),

$$f\left(x\right) = 2x\Big/C^2\exp\left(-(x/C)^2\right) \tag{7}$$

The introduction of this parameter may be also understood as replacing P_{rms} with a new parameter $P_{\mathrm{new}} = C \times P_{\mathrm{rms}}$. The parameter C was introduced to take into account the effects of finite spectral bandwidth and wave nonlinearities on the distribution of wave height (Longuet-Higgins, 1952). The value of C was determined based on the best fitting between the measured and the estimated average of n largest wave pressures obtained by modified Rayleigh distribution in section 4.3.

The two-parameter Weibull function, which is much more flexible than Eq. (7), was also applied in this study

$$f\left(x\right) = \frac{a}{\lambda}(x/\lambda)^{a-1}exp-(x/\lambda)^a \tag{8}$$

where a is the shape parameter and λ is the scaling parameter. The values of a and λ were obtained by $\overline{x} = \lambda\Gamma\left(1+\frac{1}{a}\right)$ (where Γ is the Gamma Function) by the maximum likelihood method (Saleh et al., 2012). The Weibull distribution reduces to the Rayleigh one in Eq. (6) when $\lambda = 1$ and $a = 2$, and it becomes the modified Rayleigh in Eq. (8) when $a = 2$. Thus, the classic or modified Rayleigh represents a special case of the two-parameter Weibull distribution.

4.2. Distributions of wave parameters

The field data of wave pressure P were compared with the Rayleigh, modified Rayleigh and Weibull distribution functions, respectively. The empirical probability density distribution of P is defined as

$$f_i = \frac{C_i}{N \cdot W_i} \tag{9}$$

where C_i is the number of P/P_{rms} falling into the ith bin, N is the total number of waves recorded at each of the study sites, W_i is the width of the ith bin, which was set as a constant of 0.08 to divide the P/P_{rms} range into 32 bins. Eq. (9) was also applied to calculate the empirical distribution of wave orbital velocity by replacing P/P_{rms} with U/U_{rms}. The normalized P and U by using the respective root-mean-square P_{rms} and U_{rms} would eliminate the influence of dramatic variations in the sea state during the field observations.

The probability density distributions of P/P_{rms}, and U/U_{rms}, obtained

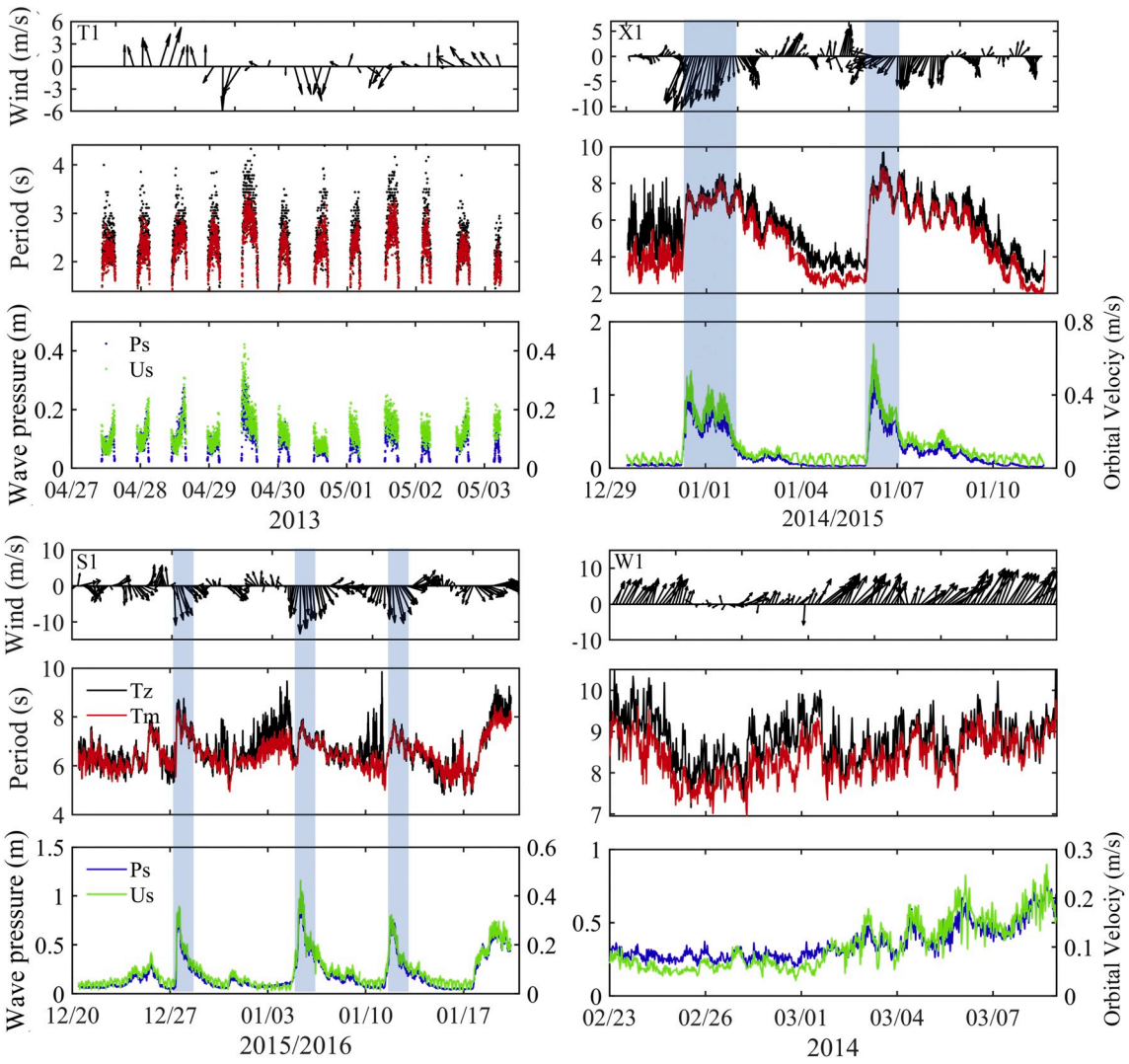

Fig. 4. *In situ* data of wind, wave period, significant wave pressure, and significant wave orbital velocity from the sites T1, X1, S1 and W1.

by the measured data, are compared against the three commonly-used distribution functions in Fig. 6 and Fig. 7, respectively. Since the distributions of P and U measured at each site have similar patterns, only the distributions of P measured at the study sites (Fig. 6) were used to discuss how the distribution varies with water depth and other related variables.

The distribution of P at the shallow site T1 of $\overline{h} = 0.8$ m is quite different from those at the other three inner shelf sites of $\overline{h} = 14.6$–27.6 m (Fig. 6): it does not follow the classic or modified Rayleigh distribution. This discrepancy may be due to the observation that the Rayleigh distribution, which is derived based on the assumption of narrow-banded waves, is no longer valid for wind-waves at this very shallow site (Kumar et al., 2011). Further, the depth-induced wave breaking can also cause wave height distribution to differ significantly from the Rayleigh (Battjes and Groenendijk, 2000; Power et al., 2016), which will be further discussed below. In contrast, the two-parameter flexible Weibull distribution agrees well with the field data collected at all other study sites, where there were wind-waves only at T1, mixed wind-waves and swells at X1, and swells only at S1 and W1.

Although the Weibull distribution agreed well with all the field data (Figs. 6 and 7), the Weibull parameters (λ, a) varied significantly with different water depths (Fig. 8). For any of the sites, the parameters λ and a in terms of the Weibull distribution were estimated from the field data at 0.1 m intervals of the local water depth change at the site T1 ($\overline{h} = 0.8$ m), and at 1.0 m intervals at the other three sites ($\overline{h} = 14.6$–27.6 m). The Weibull parameters estimated from the U data were also compared with those from the data on the perpendicular wave orbital velocity amplitudes (u, v) to verify Eqs. (3)–(5). Fig. 8 shows that the use of u, v or U is almost equally good for the estimate of the Weibull parameters; the parameters (λ, a) estimated from the U data are generally close to those from the P data, and are shown to increase with decreasing water depth, approaching to $a \approx 2$ and $\lambda = 1$ of the Rayleigh distribution at the site W1 where $\overline{h} = 27.6$ m. Elsewhere, the transition from the Rayleigh to Weibull distribution was reported also by Baquerizo and Losada (1999) under the influence of shoreward beach profile and the local relative water depth.

Due to the lack of storm event records at T1, the field observations of instantaneous wave pressure and current velocities recorded at another tidal flat site R2 (Fig. 1), which experienced strong winds with a maximum wind speed over 17 m/s, were analyzed to further study the possible effects of wave breaking and water column turbulence on the distribution of wave pressure. The probability density distribution of wave pressure was also obtained from Eqs. 1-2, and 6-9. According to Cheng and Wang (2015), turbulence kinetic energy (TKE) within the active wave breaking zone is larger than that within the non-breaking zone. The TKE was calculated by $\mathrm{TKE} = \frac{1}{2}(\overline{u'^2} + \overline{v'^2} + \overline{w'^2})$, where u', v' and w' are turbulent components in alongshore, cross-shore and vertical direction, respectively. The turbulent velocities were separated

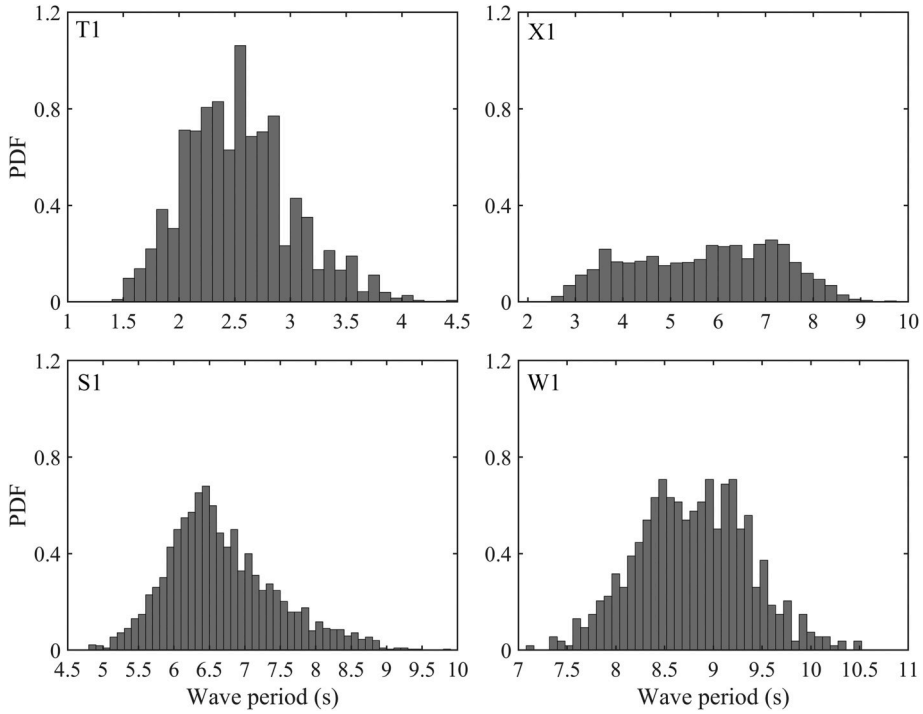

Fig. 5. Distributions of wave period $\overline{T}_z$ measured at the study sites: wind-waves with $\overline{T}_z$<5 s at the site T1 of $\overline{h}$ = 0.8 m, swell with $\overline{T}_z$>5 s at the sites S1 and W1 of $\overline{h}$ = 19.8–27.6 m, and wind-waves mixed with swell at the site X1 of $\overline{h}$ = 14.6 m.

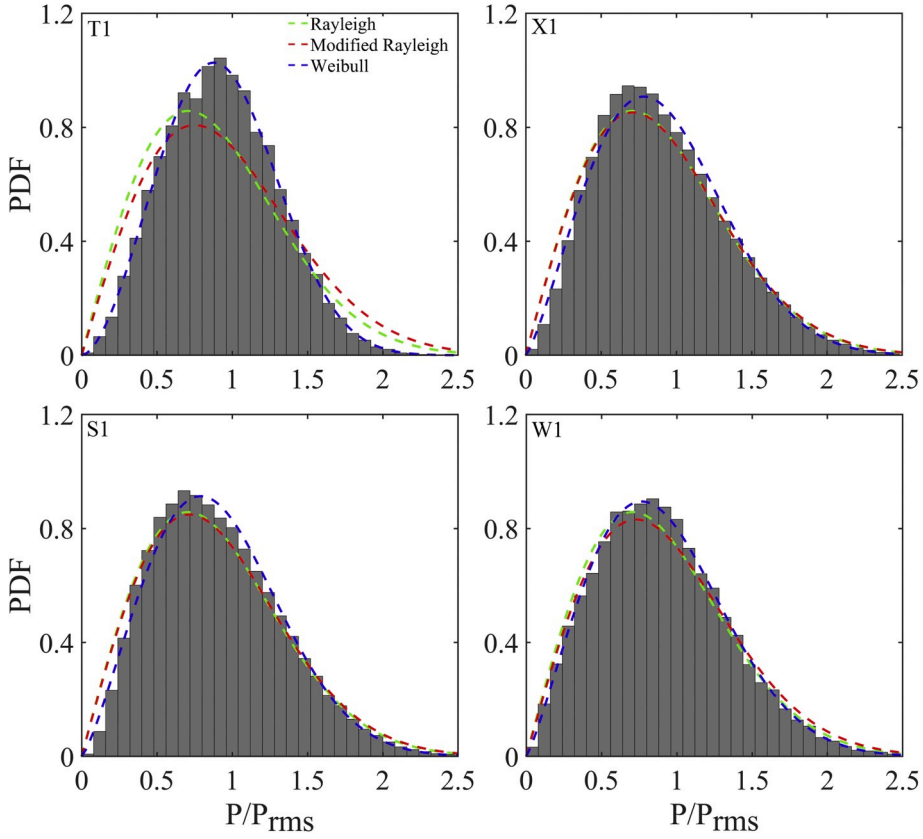

Fig. 6. Probability density distributions (PDF) of P/P_{rms} measured at the study sites of $\overline{h}$ = 0.8 m (T1), $\overline{h}$ = 14.6 m (X1), $\overline{h}$ = 19.8 m (S1)and $\overline{h}$ = 27.6 m (W1), as compared with those of the Rayleigh, modified Rayleigh and Weibull distributions.

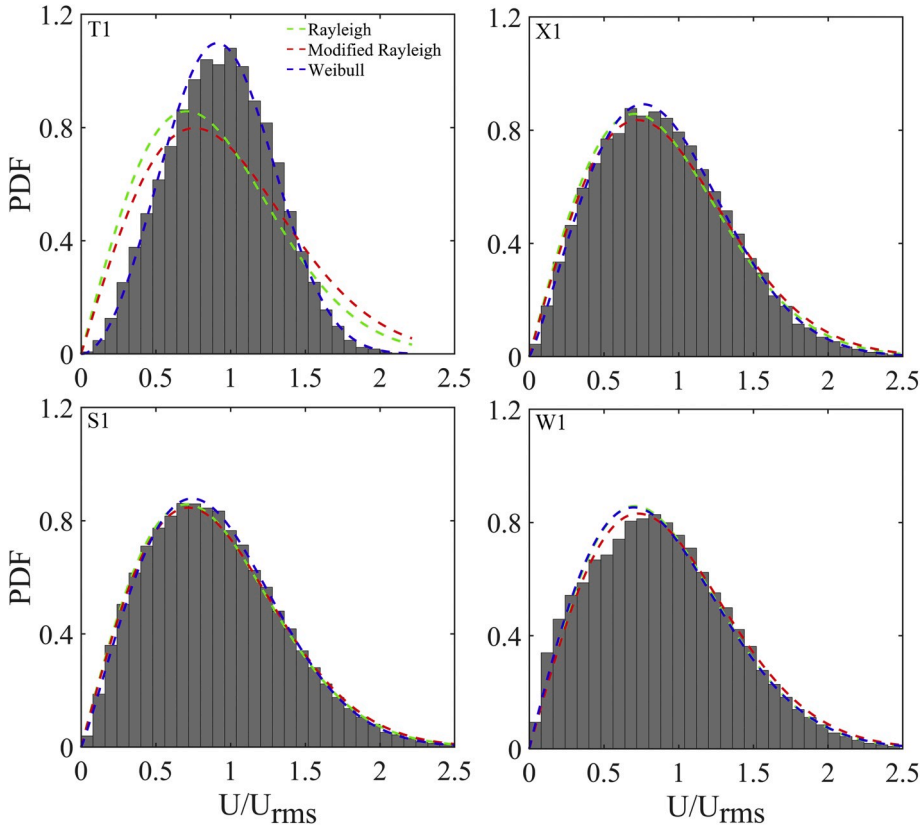

Fig. 7. Probability density distributions of U/U_{rms} measured at the study sites of $\overline{h} = 0.8$ m (T1), $\overline{h} = 14.6$ m (X1), $\overline{h} = 19.8$ m (S1) and $\overline{h} = 27.6$ m (W1), as compared with those of the Rayleigh, modified Rayleigh and Weibull distributions.

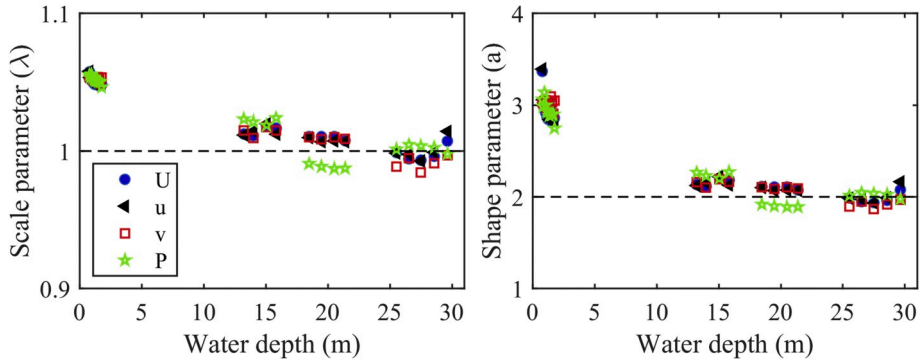

Fig. 8. Variations of the Weibull parameters (λ, a) with water depth, based on the measurements.

from the mixed wave-turbulent velocities through the "phase method" of Bricker and Monismith (2007) (MacVean and Lacy, 2014).

Fig. 9 shows that TKE increased greatly corresponding to those three tidal cycles with strong waves, with the average value of H_s being 0.49 m. The distribution of large waves ($H_s > 0.50$ m) with possible wave breaking was compared with that of small waves ($H_s < 0.15$ m) without wave breaking in Fig. 10, with the strong wave signal being shown apparently as the peak signal in the spectral density of horizontal velocity. The threshold "0.15" and "0.5" were chosen mainly based on the overall distribution of waves at site R2 (Fig. 9), such that the large and small wave groups had a comparable number of waves. In Fig. 10 the distribution of the large waves ($H_s > 0.50$ m) with possible wave breaking was almost identical to that of the small waves ($H_s < 0.15$ m) without wave breaking; the distribution of wave pressure still deviated from the Rayleigh distribution, but agreed well with the Weibull distribution. This was similar to the patterns of the site T1.

Furthermore, the influence of turbulence on wave pressure distribution was investigated (Fig. 11), based on the results of turbulence dissipation parameter $G = \left(\frac{\varepsilon}{\nu}\right)^{1/2}$, where ν is the molecular viscocity and $\varepsilon = \frac{u_*^3}{\kappa z}$ is the turbulence dissipation rate. In the equation for ε, κ (=0.4) is the von Karman constant, z is the elevation of the measurement sample volume above sea bed and u_* is the bottom shear velocity (Wang et al., 2013). The calculation of u_* is $u_* = \left(\frac{2\pi\kappa z}{\bar{u}}\right)^{1/3}\left(\frac{\varnothing_{ww}(f)f^{5/3}}{\alpha_3}\right)^{1/2}$, where $\varnothing_{ww}$ is the spectral density of vertical velocity component at the frequency f, and $\alpha_3 \approx 0.69$ (Kim et al., 2000). The strong and weak turbulence periods were defined as $G < 4\ s^{-1}$, and $G > 10\ s^{-1}$, respectively. Maximum G values during the storm event (during 15–17th October) were slightly smaller than those before the storm event (Fig. 9). Once again, the Weibull distribution was shown to agree with the measured data better

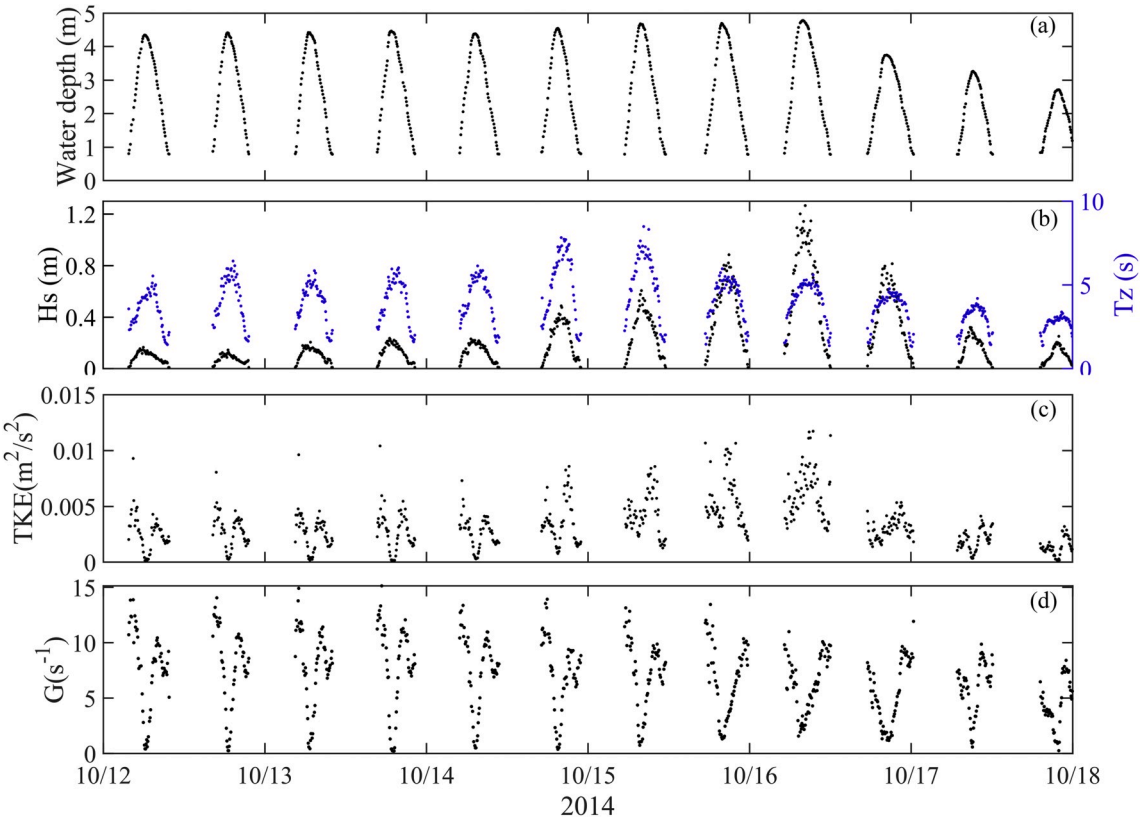

Fig. 9. Time series of (a) water depth, (b) significant wave height H_s, (c) turbulence kinetic energy TKE, and (d) turbulence dissipation parameter G, measured at the site R2.

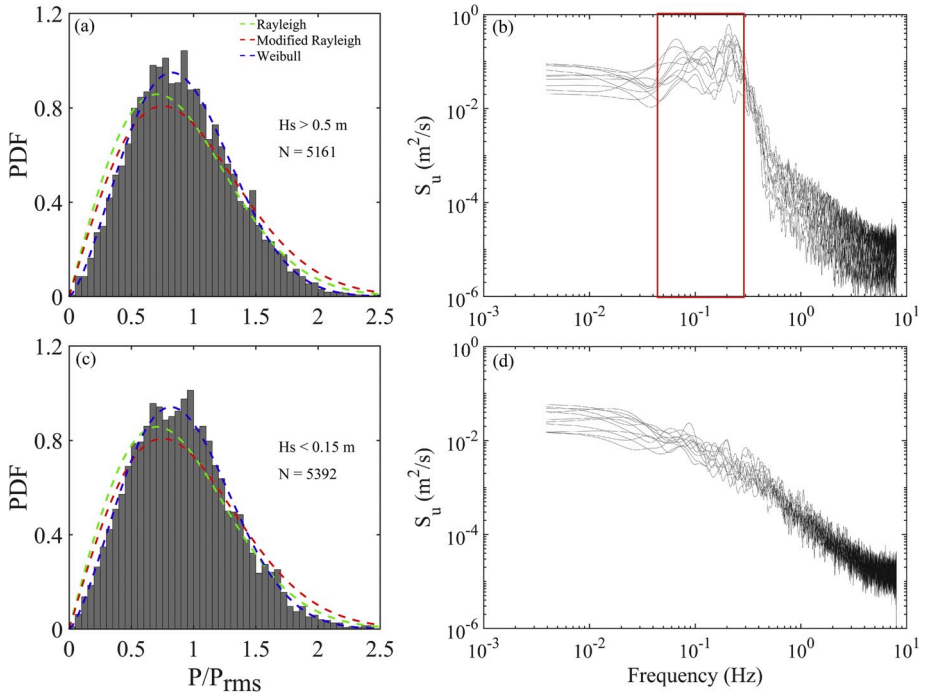

Fig. 10. Probability density distributions of P/P_{rms} measured under strong (a) and weak (c) winds at site R2, N being the number of waves in consideration, with the respective spectra of horizontal velocity (b and d). The red box denotes the wave-induced peak signal. (For interpretation of the references to colour in this figure legend, the reader is referred to the Web version of this article.)

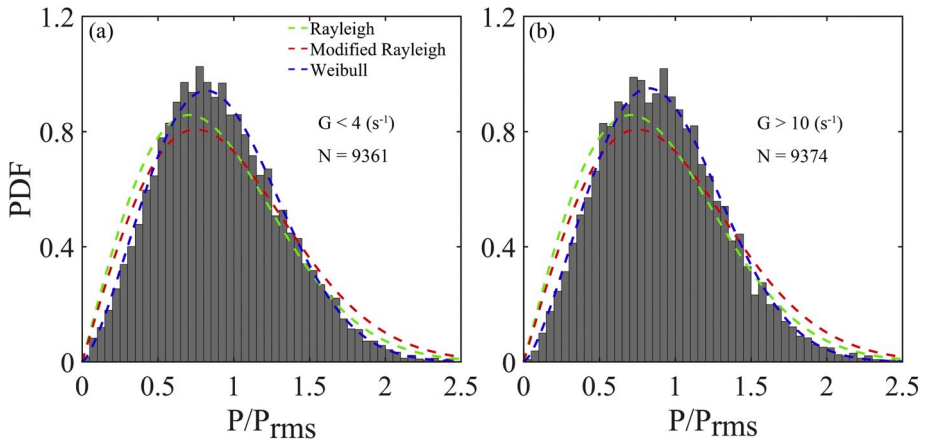

Fig. 11. Probability density distributions of P/P_{rms} measured under strong (a) and weak (b) turbulence conditions at site R2, N being the number of waves considered.

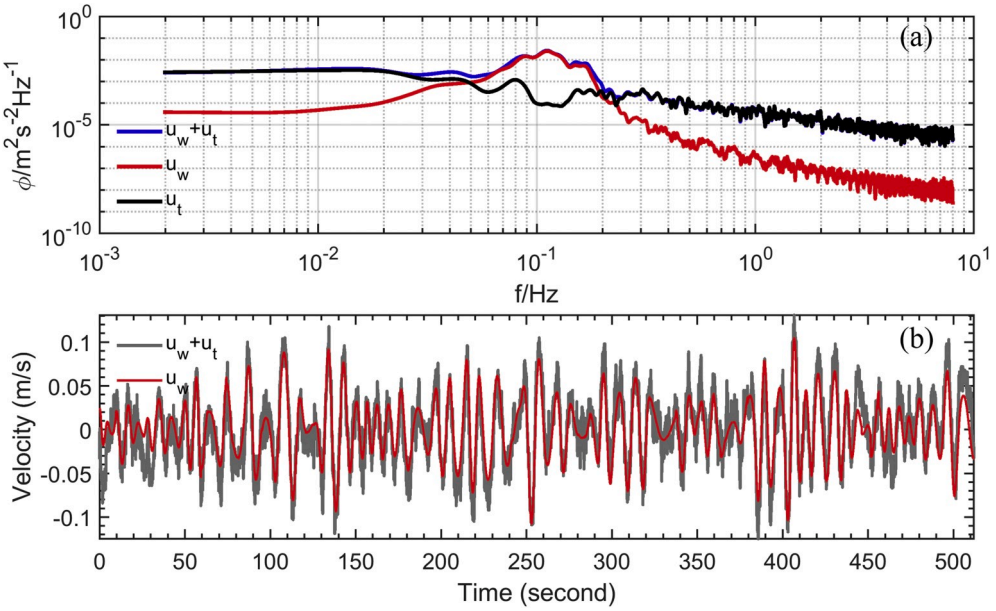

Fig. 12. Power spectra of wave orbital velocity with turbulence (blue line) and without turbulence (red line), and turbulence (black line) (a), and the time series of instantaneous wave orbital velocity with turbulence and time series of wave orbital velocity without turbulence (b). (For interpretation of the references to colour in this figure legend, the reader is referred to the Web version of this article.)

than the classic or modified Rayleigh distribution.

We further remove turbulence velocity components (u_t, v_t) from the instantaneous wave orbital velocity ($\tilde{u} = u_w + u_t$, $\tilde{v} = v_w + v_t$) by applying the Synchrosqueezed Wavelet Transform algorithm (SWT, Bian et al., 2018). Fig. 12 shows the resultant power spectra of the wave-turbulence decompositions. Part of the turbulence signals at the wave frequencies was removed with an artificial "energy trough" in the turbulence spectrum (Bian et al., 2018). The probability density distributions of u/u_{rms} from the inner shelf to the intertidal sites before and after removing turbulence are shown in Fig. 13. Minor variations were detected on the wave orbital velocity distribution at the inner shelf sites (W1, X1, and S1), while the distribution at the site R2 matched well with both Rayleigh and Weibull distributions after the removal of turbulence. Yet, at the shallowest site T1, the improvement was moderate, with the wave orbital velocity still deviating from the Rayleigh distribution; nevertheless, it followed the Weibull distribution. These observations indicate that the effect of bottom turbulence on the distribution of wave height became significant in very shallow water environments, especially when waves breaking occurred, which generated strong turbulence.

4.3. Average of n largest wave pressures

The three commonly-used probability distribution functions were used to calculate the average of n largest wave pressures or n largest wave orbital velocities measured at the study sites. Let X_Q be the average of n largest wave pressures or wave orbital velocities from the total number of m waves in a sampling burst, and $Q = n/m$ be the exceeding probability. X_Q was calculated from the Rayleigh distribution as

$$\frac{X_Q}{X_{rms}} = \frac{\int_X^\infty Xf(X)dX}{X_{rms}Q} = \sqrt{-\ln Q} + \frac{\sqrt{\pi}}{2Q} erfc\left(\sqrt{-\ln Q}\right) \tag{10}$$

where $f(X)$ is the probability density function, and *erfc* (x) is the complementary error function. Using the modified Rayleigh distribution function, X_Q became

$$\frac{X_Q}{X_{rms}} = C \times \left[\sqrt{-\ln Q} + \frac{\sqrt{\pi}}{2Q} erfc\left(\sqrt{-\ln Q}\right)\right] \tag{11}$$

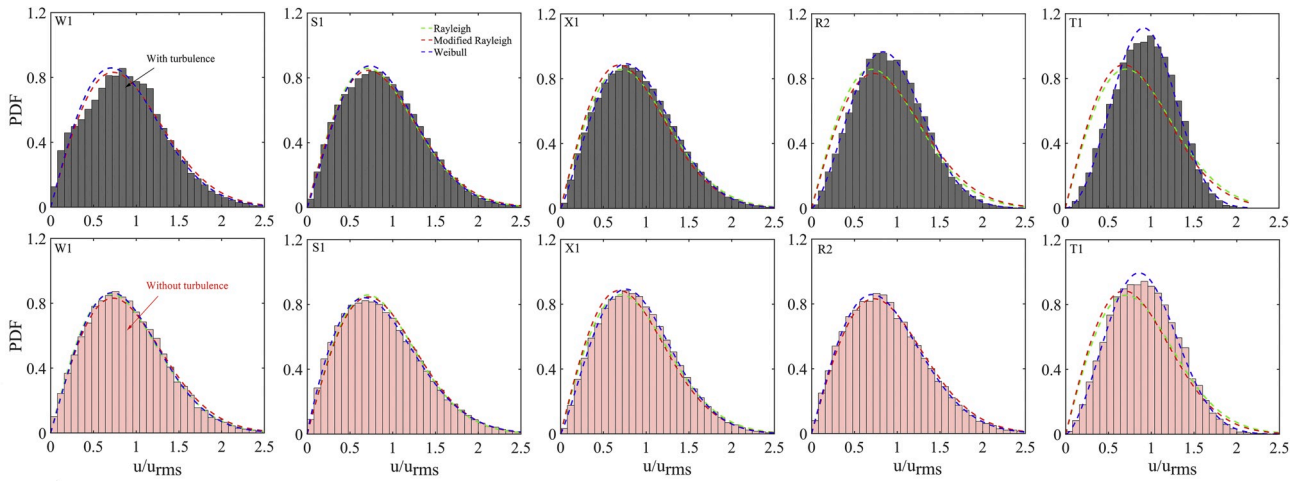

Fig. 13. Probability density distributions of wave orbital velocity amplitude with (upper panel) and without (lower panel) turbulence, from the inner shelf to intertidal sites.

For the Weibull distribution, X_Q was expressed as

$$\frac{X_Q}{X_{rms}} = (-\ln Q)^{1/\alpha} + \frac{1}{\alpha Q}\Gamma(1/\alpha, -\ln Q) \tag{12}$$

where $\Gamma(1/\alpha, -\ln Q)$ is the upper incomplete Gamma Function. The measured values of P_Q/P_{rms} at the sites were compared with those calculated from Eqs. (10-12) (Fig. 14). The U_Q distributions measured (not plotted here) were almost identical to those of P_Q as mentioned previously. The Rayleigh distribution function did not agree with the field data at the site T1, and generally overestimated the measured values at the other three sites, while the modified Rayleigh and Weibull distributions both fit well to the observations.

4.4. Expected value of wave pressure maxima

Wave pressure maxima $P_{\max}$ in different bursts or segments, with the same sample size of N waves, are expected to be different, but may follow some statistical distributions such as the Rayleigh or Weibull distribution. The expected largest value, $E(X_{max})$, in the wave burst can be estimated from the Rayleigh distribution function

$$\frac{E(X_{max})}{X_{rms}} = \chi_0 + \frac{\gamma}{2\chi_0} - \frac{\gamma^2 + \pi^2/6}{8\chi_0^3} \tag{13}$$

where $\chi_0 = \sqrt{\ln N}$ and γ (=0.5772) is Euler's constant. If the modified Rayleigh distribution function is used, then it becomes

$$\frac{E(X_{max})}{X_{rms}} = C \times \left[\chi_0 + \frac{\gamma}{2\chi_0} - \frac{\gamma^2 + \pi^2/6}{8\chi_0^3}\right] \tag{14}$$

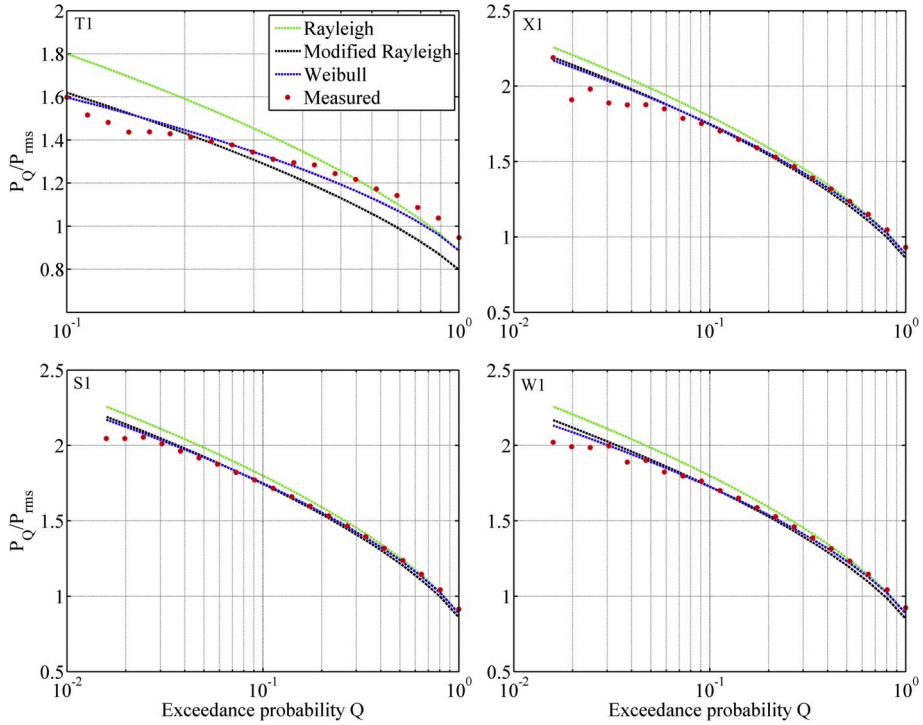

Fig. 14. P_Q/P_{rms} distributions measured in comparison with those calculated from the Rayleigh, modified Rayleigh and Weibull distributions.

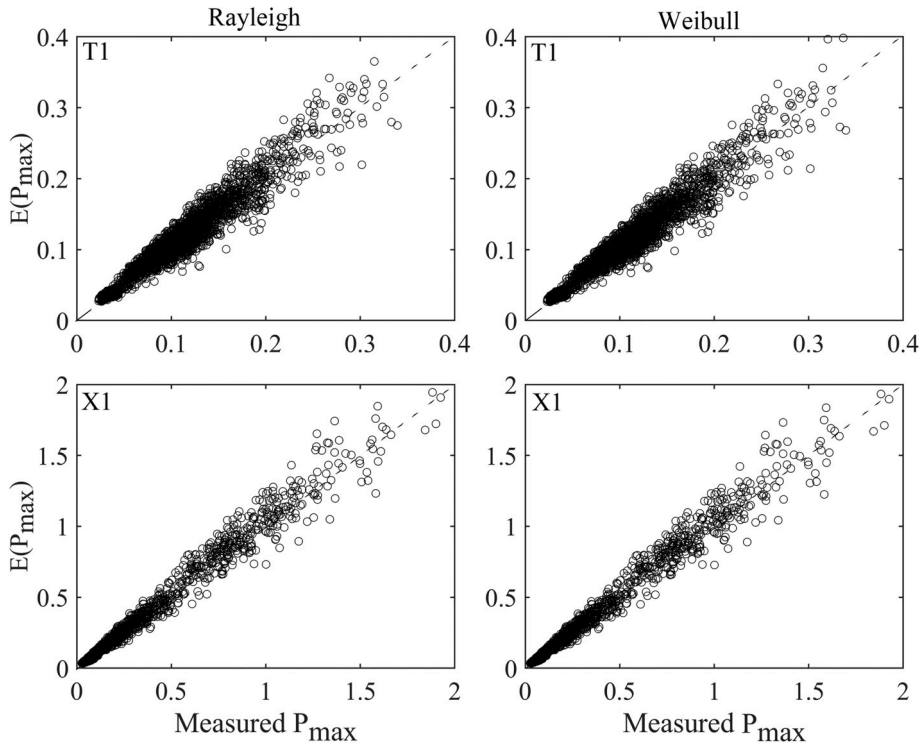

Fig. 15. Expected values calculated from the Rayleigh and Weibull distribution functions, against the measurement derived values at the sites T1 and X1.

Finally, according to the Weibull distribution function, we have

$$\frac{E(X_{max})}{X_{rms}} = \chi_0 + \frac{\gamma}{\alpha\chi_0^{\alpha-1}} - \frac{(\gamma^2+\pi^2/6)(\alpha-1)}{2\alpha^2\chi_0^{2\alpha-1}} \tag{15}$$

Comparison between the measured and predicted values of P_{max} is shown in Fig. 15. Since the measured and predicted values matched well at all study sites, only the field data collected from the intertidal sites T1 and the inner shelf site X1 are selected to make the representative comparison. The expected values of P_{max}, which are calculated from the classic Rayleigh, modified Rayleigh and Weibull distributions, are close to each other and agree well with the measured values.

5. Engineering applications

5.1. Estimation of significant wave height

For coastal engineering applications, significant wave height H_s is often estimated from the standard deviation of surface water wave profile as

$$H_s \approx 4\sqrt{m_0} \tag{16}$$

The validity of Eq. (16) relies on the precondition of a stationary, Gaussian and narrow-banded deep-water wave spectrum. Based on the field observations at the study sites, the ratios of significant wave pressure P_s to $\sqrt{m_0}$ (m_0 denotes the 0-th moment of the wave pressure spectrum) were shown to increase with water depth, approaching to the theoretical value of 4 as shown in Fig. 16. At T1 with very shallow water, however, the measured ratio is smaller than the theoretical value by 12.5%. This significant reduction is mainly due to the shallow water effect, with the presence of possible breaking waves on the tidal flat, which make the wave spectrum relatively broad banded (Kumar et al., 2011). The empirical formula, as a function of relative water depth kh, is proposed as

$$\frac{P_s}{\sqrt{m_0}} = 3.93 \times \left[1 - e^{-3.59kh}\right] \tag{17}$$

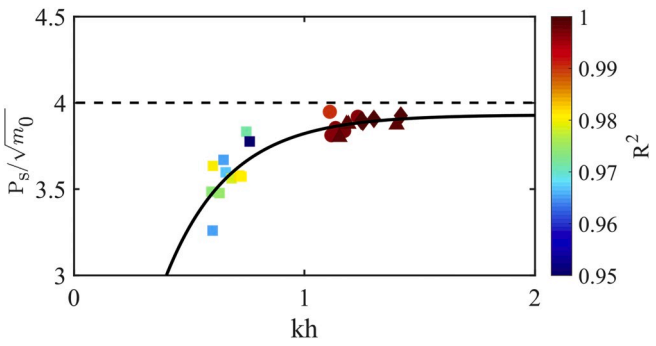

Fig. 16. The P_s to $\sqrt{m_0}$ ratio, calculated for different water depths (Squares at the site T1, Triangular shapes at the site X1, Diamonds at the site S1, and Dots at the site W1).

5.2. Applicability of the linear wave theory

In this study, the linear wave theory was used to calculate surface wave height from the wave pressure data collected *in situ*. The obtained wave heights were then compared with those measured by surface wave buoys to test the applicability of the theory in different water depths. The comparison of the significant wave heights calculated and measured at the three inner shelf sites are given in Fig. 17. It shows that the linear wave theory worked quite well in the inner shelf areas where $\bar{h}$ = 14.6–27.6 m. The wave heights calculated from the wave pressure data collected near the sea bed were close to those directly measured by the surface wave rider buoy, with some minor differences due to the error generated in the wave attenuation correction (Wang and Stone, 2005; Karimpour and Chen, 2017).

Additional tests were carried out for the intertidal site T1. With the known instantaneous wave pressure, the wave orbital velocity can be calculated from linear wave theory for monochromatic waves

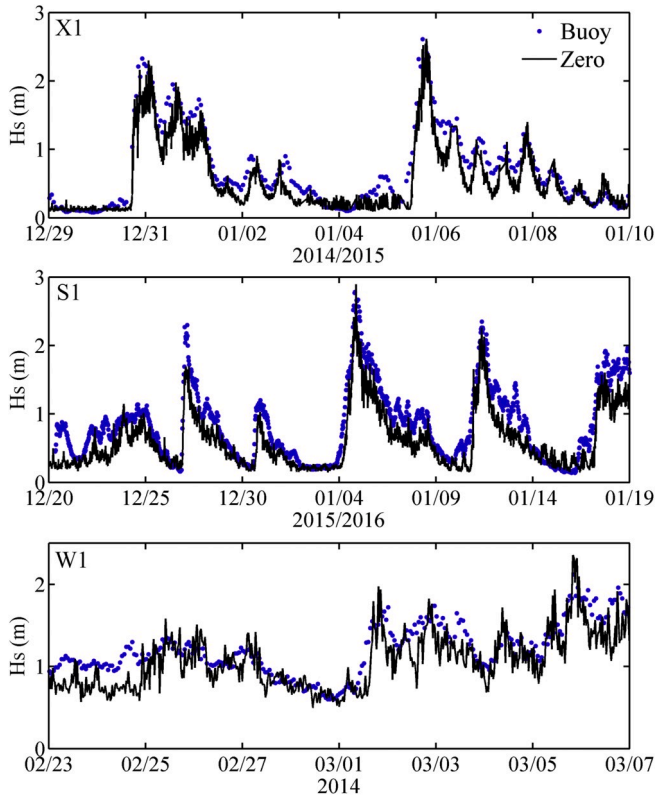

Fig. 17. Significant wave heights calculated from the wave pressure data collected at the study sites with the linear wave theory, in comparison with those on the basis of measurements by surface wave rider buoy.

$$U = \frac{\omega P}{\tanh(kh)} \tag{18}$$

for which U_{max}, P_{max} and T_z of individual waves were used, obtained from the time series of wave orbital velocity and wave pressure with the zero-up crossing method. The calculations using Eq. (18) were compared with those measured *in situ* (Fig. 18). Once again, the linear wave theory worked well at the sites of S1, X1 and W1, but the calculations were less accurate at the site T1. Since the mean value of Ursell number $U_R = \mathrm{H} \times L^2/h^3$, where H, L and h are the averaged wave height, wave length and water depth of each sampling burst, respectively, had the values of 0.36, 0.59, 0.32 and 24 for the sites W1, X1, S1 and T1, respectively (Xiong et al., 2018), the applicability of the linear wave theory was reduced at T1; this situation is associated with the large Ursell number at this particular site (i.e. $U_R \gg 1$, Ursell, 1953; Hedges and Ursell, 1995).

6. Conclusion

The effect of water depth, in association with finite-banded wave spectra, wave breaking and turbulence intensity, on the statistical distributions of wave pressure and orbital velocity amplitudes is identified in the present study, based on the *in situ* measurements carried out at two intertidal sites and three inner shelf sites. The statistical distributions obtained indicate that the two-parameter flexible Weibull distribution agrees better with the field data, than the classic or modified Rayleigh distribution does. The influences of wave breaking and the resultant turbulence on the distributions of the wave pressure and orbital velocity become important at the intertidal flat with very shallow water. Furthermore, the relationship between significant wave pressure and the 0-th moment of the wave pressure spectrum is a function of water depth within the coastal and inner shelf areas, beyond which the influence of water depth vanishes.

Declaration of competing interest

We confirm we have no conflict of interest.

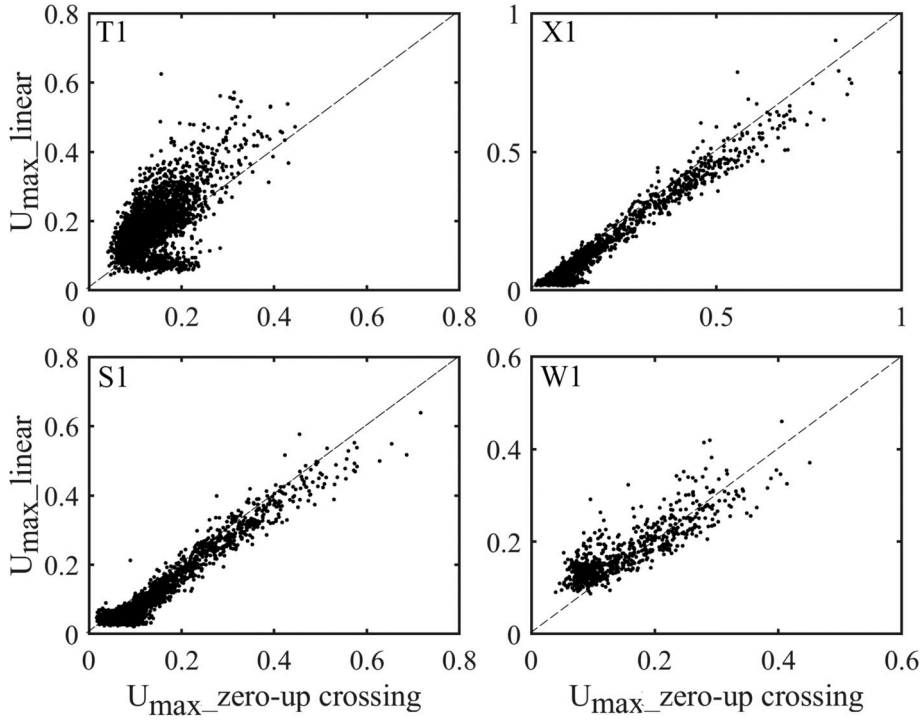

Fig. 18. Maximum wave orbital velocities of individual waves calculated from Eq. (18) based on the linear wave theory, in comparison with near-bed measurements.

CRediT authorship contribution statement

Jilian Xiong: Conceptualization, Data curation, Formal analysis, Investigation, Methodology, Validation, Visualization, Writing - original draft, Writing - review & editing. **Zai-Jin You:** Conceptualization, Funding acquisition, Methodology, Project administration, Supervision, Writing - original draft, Writing - review & editing. **Jin Li:** Formal analysis, Validation, Visualization, Software, Writing - review & editing. **Shu Gao:** Investigation, Project administration, Resources, Software, Supervision, Writing - review & editing. **Qing Wang:** Formal analysis, Validation, Visualization, Software. **Ya Ping Wang:** Conceptualization, Data curation, Funding acquisition, Investigation, Methodology, Project administration, Resources, Software, Supervision, Writing - original draft, Writing - review & editing.

Acknowledgements

This study was financially supported by the National Natural Science Foundation of China (41625021), the Laboratory for Marine Geology, Qingdao National Laboratory for Marine Science and Technology (MGQNLM-TD201807), and Innovation Program of Shanghai Municipal Education Commission (2019-01-07-00-05-E00027). You ZJ was supported by the Major Research Grant from the National Natural Science Foundation of China and the Provincial Natural Science Foundation of Shandong (Ref No: U1806227). We thank Shi BW, Chen DZ, Lu HH, Zhu QG, Cheng GL, Chen DX and Ji CC for their assistance in the field work and laboratory measurements. We also thank Qin QB who helped to improve the manuscript. Finally, we wish to thank the two anonymous reviewers who helped to greatly improve the manuscript.

Appendix A. Supplementary data

Supplementary data to this article can be found online at https://doi.org/10.1016/j.coastaleng.2020.103714.

References

Baquerizo, A., Losada, M.A., 1999. Wave height to depth ratio in front of coastal structures. Proc. Coast. Struct. 99, 23–28. Balkema, Rotterdam (2000).
Battjes, J.A., 1974. Computation of Set-Up, Longshore Currents, Run-Up and Overtopping Due to Wind-Generated Waves. Department of Civil Engineering, Delft University of Technology, Netherlands (Ph.D. dissertation).
Battjes, J.A., Groenendijk, H.W., 2000. Wave height distributions on shallow foreshores. Coast. Eng. 40 (3), 161–182.
Bian, C., Liu, Z., Huang, Y., Zhao, L., Jiang, W., 2018. On estimating turbulent Reynolds stress in wavy aquatic environment. J. Geophys. Res.: Oceans 123 (4), 3060–3071.
Bricker, J.D., Monismith, S.G., 2007. Spectral wave–turbulence decomposition. J. Atmos. Ocean. Technol. 24 (8), 1479–1487.
Cartwright, D.E., Longuet-Higgins, M.S., 1956. The statistical distribution of the maxima of a random function. Proc. R. Soc. Lond. Ser. A 247, 22–48.
Cheng, J., Wang, P., 2015. Extracting turbulence under breaking waves in the surf zone. J. Waterw. Port, Coast. Ocean Eng. 141 (6), 06015003.
Dally, W.R., 1990. Random breaking waves: a closed-form solution for planar beaches. Coast. Eng. 14 (3), 233–263.
Dally, W.R., 1992. Random breaking waves: field verification of a wave-by-wave algorithm for engineering application. Coast. Eng. 16 (4), 369–397.
Ding, X., Kang, Y., Mao, Z., Su, Y., Li, S., Gao, X., Zhao, X., 2014. Analysis of largest tidal sand ridges southern Yellow Sea. Acta Oceanol. Sin. 36 (11), 12–20 (In Chinese, with English abstract).
Dong, L.X., Guan, W.B., Chen, Q., Li, X.H., Liu, X.H., Zeng, X.M., 2011. Sediment transport in the Yellow Sea and East China sea. Estuar. Coast Shelf Sci. 93 (3), 248–258.
Du, P., Hu, K., Kong, Y., Ding, P., 2007. Application of ECOMSED model to the simulationof Hangzhou Bay tide current. Acta Oceanol. Sin. 29 (1) (In Chinese, with English abstract).
Elfrink, B., Hanes, D.M., Ruessink, B.G., 2006. Parameterization and simulation of near bed orbital velocities under irregular waves in shallow water. Coast. Eng. 53 (11), 915–927.
Forristall, G.Z., 1978. On the statistical distribution of wave heights in a storm. J. Geophys. Res. 83, 2353–2358.
Glukhovskiy, B.K., 1966. Investigation of sea wind waves. In: Leningrad, Gridrometeo-Izdat (Reference Obtained from E. Bouws. Spectra of Extreme Wave Conditions in the Southern North Sea Considering the Influence of Water Depth): Proc. Of Sea Climatology Conf, pp. 51–71. Paris.
Goda, Y., 2010. Reanalysis of regular and random breaking wave statistics. Coast Eng. J. 52, 71–106, 01.
Goring, D.G., Nikora, V.I., 2002. Despiking acoustic Doppler velocimeter data. J. Hydraul. Eng. 128 (1), 117–126.
Hedges, T.S., Ursell, 1995. Regions of validity of analytical wave theories. Proc. Ins. Civ. Eng. -Water Marit. Energy 112 (2), 111–114.
Jadhav, R.S., Chen, Q., 2013. Probability distribution of wave heights attenuated by salt marsh vegetation during tropical cyclone. Coast. Eng. 82, 47–55.
Karimpour, A., Chen, Q., 2017. Wind wave analysis in depth limited water using OCEANLYZ, A MATLAB toolbox. Comput. Geosci. 106, 181–189.
Kim, S.C., Friedrichs, C.T., Maa, J.Y., Wright, L.D., 2000. Estimating bottom stress in tidal boundary layer from acoustic Doppler velocimeter data. J. Hydraul. Eng. 126 (6), 399–406.
Kumar, V.S., Singh, J., Pednekar, P., Gowthaman, R., 2011. Waves in the nearshore waters of northern Arabian Sea during the summer monsoon. Ocean. Eng. 38 (2–3), 382–388.
Lee, H.J., Liu, K.K., 2013. Tidal effects on changjiang plume dispersal in the East China sea. J. Mar. Sci. Technol. 21 (3), 342–352.
Liu, Z., 1982. Distribution of surface sediments in the Yellow Sea. Mar. Sci. Bull. 1 (1), 47–55 (In Chinese, with English abstract).
Longuet-Higgins, M.S., 1952. On the statistical distribution of the heights of sea waves. J. Mar. Res. 11, 245–266.
Lu, Y.Z., Wu, J.X., Liu, H., 2012. An integrated post-processing technique for turbulent flows in estuarine bottom boundary layer. Acta Oceanol. Sin. 34 (5), 39–49 (in Chinese with English abstract).
MacVean, L.J., Lacy, J.R., 2014. Interactions between waves, sediment, and turbulence on a shallow estuarine mudflat. J. Geophys. Res.: Oceans 119 (3), 1534–1553.
Mai, S., Wilhelmi, J., Barjenbruch, U., 2011. Wave height distributions in shallow waters. Coast. Eng. Proc. 1 (32), 63.
Massel, S.R., Sobey, R.J., 2000. Distribution of the highest wave in a record. Coast Eng. J. 42, 153–173, 02.
Power, H.E., Nielsen, P., Hughes, M.G., Aagaard, T., Baldock, T.E., 2016. Wave height distributions in the surf zone on natural beaches. J. Coast Res. 75 (sp1), 917–922.
Saleh, H., Aly, A.A.E.A., Abdel-Hady, S., 2012. Assessment of different methods used to estimate Weibull distribution parameters for wind speed in Zafarana wind farm, Suez Gulf, Egypt. Energy 44 (1), 710–719.
Silva, P.G., Klein, A.H., González, M., Gutierrez, O., Espejo, A., 2015. Performance assessment of the database downscaled ocean waves (DOW) on Santa Catarina coast, South Brazil. An Acad. Bras Ciências 87 (2), 623–634.
Sultan, N.J., 1992. Irregular Wave-Induced Velocity in Shallow Water. US Army Corps of Engineering, Washington DC. Technical Report CERC-92-9.
Ursell, F., 1953. The long-wave paradox in the theory of gravity waves. In: Mathematical Proceedings of the Cambridge Philosophical Society. Cambridge University Press, pp. 685–694. Vol. 49, No. 4.
van Vledder, G.P., 1991. Modification of the Glukhovskiy Distribution. Delft Hydraulics Report H, p. 1203.
Wang, P., Stone, G.W., 2005. Nearshore wave measurement. In: Schwartz, M.L. (Ed.), Encyclopedia of Coastal Science. Encyclopedia of Earth Science Series. Springer, Dordrecht.
Wang, Y.P., Voulgaris, G., Li, Y., Yang, Y., Gao, J., Chen, J., Gao, S., 2013. Sediment resuspension, flocculation, and settling in a macrotidal estuary. J. Geophys. Res.: Oceans 118 (10), 5591–5608.
Wiberg, P.L., Sherwood, C.R., 2008. Calculating wave-generated bottom orbital velocities from surface-wave parameters. Comput. Geosci. 34 (10), 1243–1262.
Wu, Y., Randell, D., Christou, M., Ewans, K., Jonathan, P., 2016. On the distribution of wave height in shallow water. Coast. Eng. 111, 39–49.
Xing, F., Wang, Y.P., Wang, H.V., 2012. Tidal hydrodynamics and fine-grained sediment transport on the radial sand ridge system in the southern Yellow Sea. Mar. Geol. 291, 192–210.
Xiong, J., Wang, Y.P., Gao, S., Du, J., Yang, Y., Tang, J., Gao, J., 2018. On estimation of coastal wave parameters and wave-induced shear stresses. Limnol Oceanogr. Methods 16 (9), 594–606.
Yang, B., Feng, W.B., Zhang, Y., 2014. Wave characteristics at the south part of the radial sand ridges of the southern Yellow Sea. China Ocean Eng. 28 (3), 317–330.
You, Z.J., 2008. A close approximation of wave dispersion relation for direct calculation of wavelength in any coastal water depth. Appl. Ocean Res. 30 (2), 113–119.
You, Z.J., 2009. The statistical distribution of nearbed wave orbital velocity in intermediate coastal water depth. Coast. Eng. 56 (8), 844–852.
You, Z.J., Chen, C., 2018. Chapter 7: coastal dynamics and sediment resuspension in laizhou Bay. In: Wang, X.H. (Ed.), Book on Sediment Dynamics of Chinese Muddy Coasts and Estuaries: Physics, Biology and Their Interactions. Elsevier Publisher.
You, Z.J., Yin, B.S., 2001. Determination of Coastal Wave Direction in Shallow Water. In: 15th Australian Coastal and Ocean Engineering Conference, pp. 523–527. Gold Coast.
Yu, Q., Wang, Y., Shi, B., Wang, Y.P., Gao, S., 2017. Physical and sedimentary processes on the tidal flat of central Jiangsu coast, China: headland induced tidal eddies and benthic fluid mud layers. Continent. Shelf Res. 133, 26–36.